SEPTEMBER 16 2025

Non-linear coupling in two non-linear delayed acoustic resonators[a)]

Jana Reda; Mathias Fink ; Fabrice Lemoult

J. Acoust. Soc. Am. 158, 2130–2137 (2025)
https://doi.org/10.1121/10.0038955

JASA ARTICLE

Non-linear coupling in two non-linear delayed acoustic resonators[a)]

Jana Reda, Mathias Fink, and Fabrice Lemoult[b)]
Institut Langevin, ESPCI Paris, Université PSL, CNRS, 75005 Paris, France

ABSTRACT:
Building on our previous work on a Hopf resonator that mimics the cochlear amplifier from Reda, Fink, and Lemoult [(2023). Europhys. Lett. **144**(3), 37001], we now turn to the fact that the inner ear comprises thousands of such resonators, which interact through coupling mechanisms. To gain insight into these interactions, we investigate the coupling of two acoustic resonators with slightly detuned resonance frequencies, interacting through time-delayed feedback loops. By modulating the gain of the loop and the coupling strength, we demonstrate the emergence of frequency synchronization at low amplitudes and bifurcations leading to desynchronization at higher amplitudes. This tunable non-linear interaction offers insights into resonance phenomena in coupled systems, with potential implications for auditory modeling and complex acoustic systems.
 https://doi.org/10.1121/10.0038955
(Received 14 March 2025; revised 13 June 2025; accepted 17 July 2025; published online 16 September 2025)
[Editor: Michael R. Haberman] Pages: 2130–2137

I. INTRODUCTION

The study of resonances is fundamental to advancing our understanding of a wide range of wave-based physical, biological, and engineering phenomena (Hamilton, 1986). For example, in the field of metamaterials, the introduction of sub-wavelength resonators has proven to be a powerful approach for shaping dispersion relations and engineering unique wave propagation properties (Lemoult *et al.*, 2011; Brunet *et al.*, 2015; Cummer *et al.*, 2016; Craster, 2024). Furthermore, by introducing a gradient in resonance frequencies, via detuning, it is possible to design gradient-index media, which have enabled effects such as rainbow trapping (Zhu *et al.*, 2013; Ni *et al.*, 2014; Tian and Yu, 2017) and perfect absorption (Jiménez *et al.*, 2017; Meng *et al.*, 2020), to cite only a few examples. These phenomena arise from multiple scattering and thus rely on the coupling between resonators, despite the subwavelength scales at play (Kaina *et al.*, 2015; Lemoult *et al.*, 2016).

However, these approaches remain within the framework of linear physics. Introducing active and non-linear mechanisms brings us closer to biological and living systems (Plaçais *et al.*, 2009; Crauste, 2009; Marsden and McCracken, 2012). In a previous work, we explored how a single nonlinear delayed resonator operating near a Hopf bifurcation can act as a cochlear amplifier (Reda *et al.*, 2023). More broadly, based on the work of Duke and Jülicher (2003), a full cochlear wave model requires an array of Hopf resonators with a gradient in their properties. Additionally, we demonstrate in a separate experiment (Rupin *et al.*, 2019) that a set of such nonlinear resonators, distributed in frequency, could reproduce key features of cochlear wave amplification at low amplitudes.

Here, we investigate the non-linear coupling between two Hopf resonators with slightly detuned frequencies, interacting through time-delayed feedback loops. Non-linear delayed feedback is known to induce a bifurcation: as the loop gain increases, a stable fixed point loses stability and self-sustained oscillations emerge (Rupin *et al.*, 2019; Reda *et al.*, 2023). Each resonator in our setup is independently programmed to operate near a Hopf bifurcation by carefully adjusting the dependence on the intensity. We demonstrate that when the coupling coefficient α reaches its maximum, the resonators synchronize and converge toward almost a common limit cycle whose amplitude matches that of the uncoupled Hopf oscillation. The system can therefore be modeled as a pair of coupled Hopf resonators. In this framework, we examine how non-linearity influences the amplification gain—defined as the system's ability to enhance the input signal—and the resonance frequencies of the coupled system. Our goal is to elucidate the mechanisms driving their interaction. This study provides valuable insight into the dynamics of coupled non-linear resonators, akin to Gomez *et al.* (2016), with potential implications for auditory modeling, metamaterials, and complex wave-based systems.

While Gomez *et al.* (2016) studied injective coupling with enhanced amplification, our system uses diffusive, time-delayed feedback, which stabilizes dynamics and delays self-oscillations. Unlike the sharper response from injective coupling, our scheme produces distinct dynamics. Yet, in both cases, signal-coupled subthreshold Hopf-type systems show a collective response.

We begin by presenting the experimental and theoretical frameworks governing the dynamics of two coupled

[a)]This paper is part of a special issue on Active and Tunable Acoustic Metamaterials.
[b)]Email: fabrice.lemoult@espci.fr

https://doi.org/10.1121/10.0038955

Hopf resonators, detailing the mathematical models and assumptions underlying our study. Subsequently, we describe the experimental setup, emphasizing the implementation of time-delayed feedback loops and the methods employed to achieve precise frequency detuning between the resonators. Our results section then elucidates the observed phenomena, including the merging of resonance frequencies at low excitation amplitudes, as well as the modulation of system gain in response to varying coupling strengths and the constant gain of each resonator.

II. EXPERIMENT

A. Experimental design

Our experiment, illustrated in Fig. 1, consists of coupling two Hopf resonators to investigate their nonlinear interactions. To achieve this, we build upon the design introduced in Reda *et al.* (2023), where a single quarter-wavelength acoustic resonator was rendered nonlinear via a feedback loop. Each resonator consists of a 1-cm-diameter Plexiglas tube, closed at one end and open at the other. The

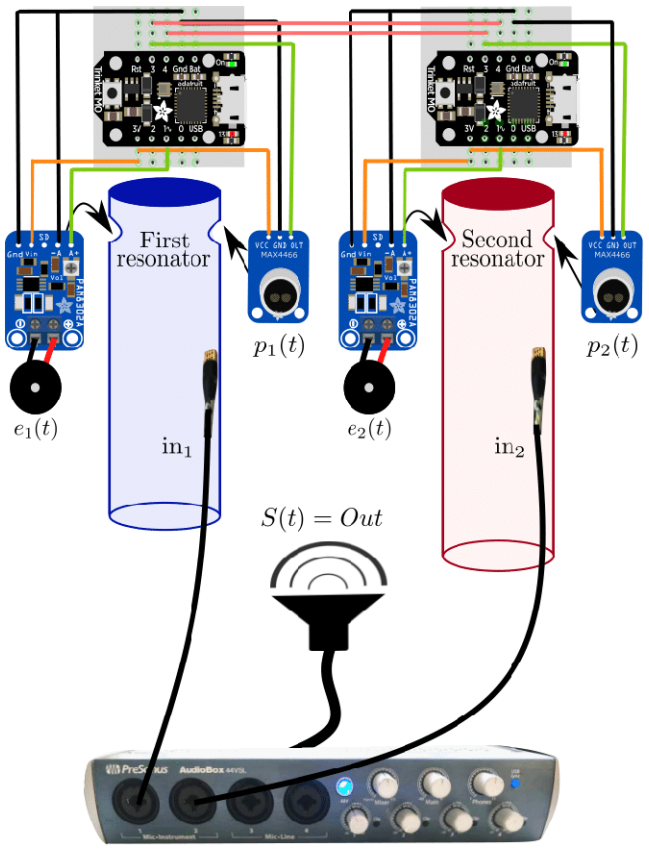

FIG. 1. Two quarter-wavelength acoustic resonators are converted into two coupled nonlinear delayed resonators. A 9-cm blue Plexiglas tube is placed next to a 9.5-cm red Plexiglas tube, both terminated by three-dimensional-printed caps. The microcontrollers (Adafruit Trinket M0, Adafruit, New York) create a feedback loop between the microphones and the speakers, while additional reddish-pink wired connections between the microcontrollers enable coupling. Measurements inside the tubes are taken using two electret microphones connected to an external soundboard (PreSonus 44VSL, PreSonus, Baton Rouge, LA).

nonlinearity is introduced through a real-time feedback mechanism: a microcontroller processes the acoustic signal captured by a microphone inside the resonator and injects a modified response via a speaker. This setup allows precise control over the gain and nonlinearity applied to the system.

In the present study, rather than working with a single nonlinear resonator, we fabricate two such resonators and introduce coupling between them. The first resonator is 9 cm long, while the second, slightly longer, measures 9.5 cm, leading to a small detuning between their resonance frequencies. Instead of relying on physical coupling, we leverage the digital processing capabilities of our setup by coupling the resonators via their microcontrollers, where the microphone of the first resonator is connected to the analog read pin of the second resonator, and vice versa. This way, each microcontroller now not only processes its own resonator's signal but also reads the signal from the neighboring resonator, enabling controlled interaction. This coupling is achieved through additional wired connections, represented by the reddish-pink lines in Fig. 1.

From a mathematical point of view, the pressure field $p_i(t)$ near the closed end of each resonator is governed by

$$p_i''(t) + \frac{\omega_i}{2Q_i} p_i'(t) + \omega_i^2 p_i(t) = S(t) + e_i(t), \tag{1}$$

where i indexes the resonators (1 or 2), ω_i denotes their natural resonance frequencies, and Q_i is their quality factors. The term $S(t)$ represents an external excitation applied via a speaker near the open ends, while $e_i(t)$ accounts for the feedback-induced source term. In this study, the feedback incorporates both the self-interaction within each resonator and the coupling to its neighbor. Given the inherent delays τ_i introduced by the analog-to-digital conversion and processing, $e_i(t)$ takes the form

$$e_i(t) = f(p_i(t-\tau_i), p_j(t-\tau_i)), \tag{2}$$

where j refers to the neighboring resonator, and f is a nonlinear function that determines the relative contribution of self-feedback and cross-feedback from the two resonators. By tuning the function f, we aim to reproduce the key characteristics of systems operating near a Hopf bifurcation, including nonlinear amplitude compression near resonance, frequency selectivity with sharp tuning, and such behaviors typical of systems near a Hopf bifurcation (Duke and Jülicher, 2003; Rupin *et al.*, 2019; Reda *et al.*, 2023), while also introducing nonlinear coupling between the two resonators.

Before introducing the coupling, we first need to calibrate the response of each individual resonator to be linearly active. We start by selecting a feedback function f that depends only on the acoustic field within the same resonator and with a constant gain,

$$e_i(t) = G_i p_i(t-\tau_i). \tag{3}$$

With this choice of feedback function, the system's behavior is governed by two key parameters: the delay τ_i

and the gain G_i. As described in a previous work (Reda *et al.*, 2023), when G_i exceeds a critical threshold, the feedback loop compensates for the intrinsic losses of the system, leading to an exponential increase in amplitude and ultimately resulting in self-sustained oscillations of the resonator, indicating a linear instability. Conversely, when G_i remains below this threshold, the losses dominate, and the feedback is insufficient to maintain oscillations. To ensure stable operation, we must carefully determine the operating point of our resonators by appropriately setting both the delay and this constant gain.

The total delay in the system arises from the analog-to-digital conversion, digital processing, and digital-to-analog conversion within the microcontroller. In addition to these inherent delays, we can introduce an adjustable software delay, corresponding to different sampling intervals within the microcontroller. Given the 48 kHz sampling frequency, the system's time resolution is approximately $\delta t = 21\ \mu$s. To select an appropriate delay, we define it as the smallest software delay $\tau_s = N\,\delta t$, with N an integer, for which the oscillation frequency just above the critical gain matches the resonator's passive resonance frequency. Increasing N gradually increases the software delay, allowing fine-tuning of the oscillation frequency until it matches the natural resonance frequency ω_i. The minimum possible software delay yields $36\,\delta t$ for the first resonator, corresponding to $f_1 = 973$ Hz, and $4\,\delta t$ for the second resonator, corresponding to $f_2 = 907$ Hz.

Once the delay is established, we determine an appropriate constant gain G_i by applying short pulses at the natural frequency ω_i of each resonator. The gain of each resonator must remain below the critical threshold; exceeding this value would cause self-sustained oscillations. To maximize the response while avoiding instability, we select the highest gain values that do not trigger sustained oscillations. This leads to final values of $G_1 = 1$ and $G_2 = 1.18$ in the software, with comparable amplifier gains in both feedback loops.

After calibrating the system, we introduce two key modifications: (i) introducing nonlinearity to study resonators operating near a Hopf bifurcation, and (ii) adding a coupling term to investigate the behavior of two coupled nonlinear resonators. To understand how a single cubically nonlinear delayed acoustic resonator (Reda *et al.*, 2023) behaves when coupled with a second one, we first reintroduce the same cubic nonlinear gain as originally proposed. The transition between low- and high-amplitude oscillations follows a cubic nonlinearity (Nin *et al.*, 2012), which leads to a variation in the resonator's quality factor with excitation amplitude, thereby amplifying low-amplitude signals. To account for coupling, we modify the gain function f to numerically link the resonators in real time via the microcontrollers. So it is now modified to include Y_i, the coupled pressure in resonator i:

$$Y_i(t) = \alpha p_j(t-\tau_i) + (1-\alpha)p_i(t-\tau_i). \tag{4}$$

The parameter α controls the balance between self-feedback (p_i) and cross-feedback (p_j), effectively setting the strength of the coupling. When $\alpha = 0$, resonator i relies entirely on its own feedback; when $\alpha = 1$, it depends only on the neighboring resonator j. Intermediate values of α between 0 and 1 represent a mixture of the two.

As a result, each resonator now operates with its own loop function $e_i(t)$, and dynamically controls the feedback according to

$$e_i(t) = \begin{cases} G_i Y_i(t)\left(1 - \left(\dfrac{Y_i(t)}{P_0}\right)^2\right) & \text{if } |Y_i(t)| < P_0, \\ 0 & \text{otherwise.} \end{cases} \tag{5}$$

Here, P_0 defines the amplitude threshold above which the gain is turned off, while $Y_i(t)$ in Eqs. (4) and (5) represents the delayed self- and cross-feedback pressure input, which shapes the nonlinear response.

B. Experimental method

The experiment then consists of emitting monochromatic sound waves for one second using an external loudspeaker and measuring the pressure inside the tubes with electret microphones connected to the soundboard (see Fig. 1). For each excitation, we analyze only the system's response at the same frequency as the excitation by performing a Fourier transform on the recorded time-domain signal and retaining only the coefficient corresponding to the chosen frequency. These measurements are conducted while varying both the excitation amplitude and the frequency around f_1 and f_2. The entire procedure is then repeated for different values of the coupling parameter α.

III. RESULTS

Results for three different values of α are summarized in Figs. 2(a)–2(c), where the raw data are represented, with the signal from resonator 1 shown in blue and the signal from resonator 2 in red. The intensity of the color indicates the amplitude, with lighter colors corresponding to lower excitation levels and gradually transitioning to darker colors as the excitation increases. By extracting the maximum value of these curves for each resonator, we construct the corresponding sensitivity curves in Figs. 2(d)–2(f), which reveal the maximum response of each resonator as a function of the excitation amplitude. It is important to note that the definition of decibels here is arbitrary and does not correspond to absolute sound pressure levels. Instead, we use normalized units, setting 0 dB as the reference for the maximum recorded measurement.

For $\alpha = 0$, meaning there is no coupling, we analyze the experimental results shown in Figs. 2(a) and 2(d). Starting with Fig. 2(a) at low excitation amplitudes (light red and blue), both resonators exhibit sharp frequency responses, indicative of high-quality factors. This behavior is expected, as for small pressure amplitudes $|Y_i(t)| \ll P_0$, so following our definition for the gain, Eq. (5), it remains

https://doi.org/10.1121/10.0038955

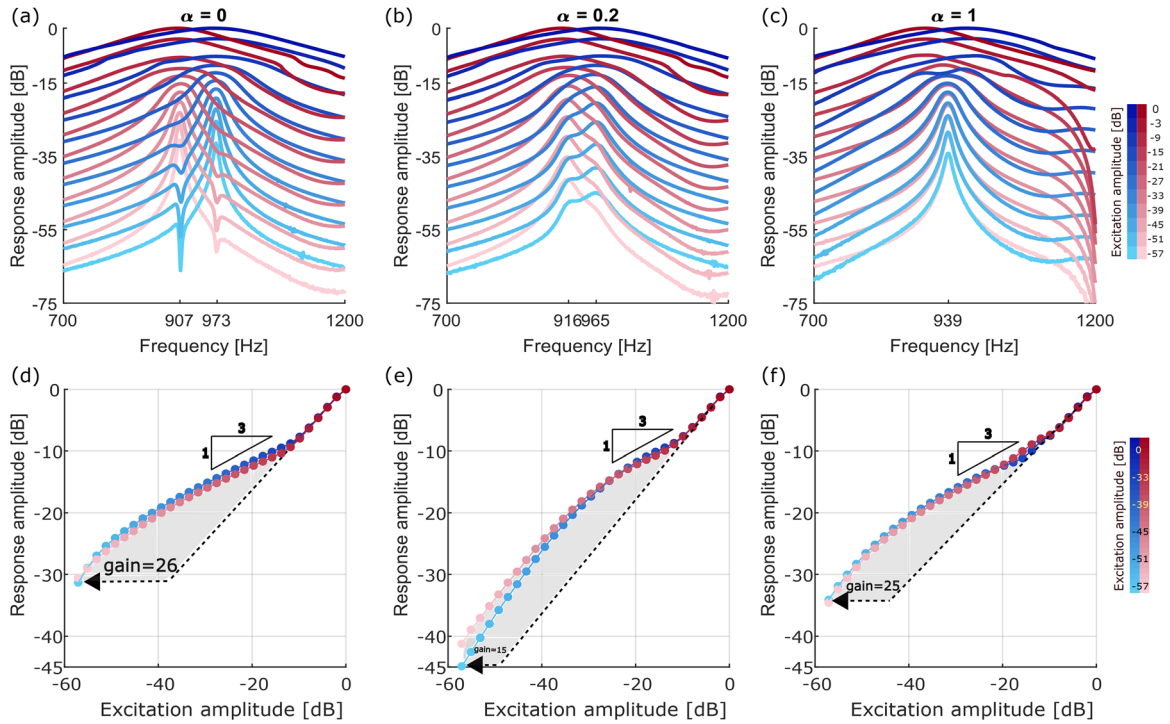

FIG. 2. Active resonators transition from an uncoupled state to maximum coupling near a Hopf bifurcation. Figures (a)–(c) show the frequency response of resonator 1 (blue) and resonator 2 (red) for various excitation amplitudes, with lighter colors indicating lower amplitudes. In (a), with no coupling ($\alpha = 0$), the resonators oscillate at their uncoupled natural frequencies. As the coupling increases to $\alpha = 0.2$ in (b), their frequencies begin to converge. At $\alpha = 1$ in (c), they fully merge into a single synchronized response at 939 Hz. Figures (d)–(f) present the corresponding sensitivity curves, obtained by retaining only the maximum response at each excitation amplitude revealing three distinct response regimes: linear, inverse cubic, and linear again. These curves correspond to the same experimental conditions as (a)–(c), respectively. The gray-shaded region highlights the gain.

close to its nominal value G_i, ensuring sustained amplification near the bifurcation. Consequently, the resonance peak is well defined and located near the expected eigenfrequency of the resonator.

As the excitation amplitude increases (the shades of red and blue gradually become darker), we observe a progressive broadening and flattening of the resonance peak. This trend corresponds to a gradual reduction in the signal injected into the loop, following the cubic dependence on instantaneous pressure. At very high amplitudes $|Y_i(t)| \gg P_0$, the gain effectively drops to zero, and the resonators behave as passive quarter-wavelength resonators with significantly lower quality factors. In this regime, the resonance peaks become much less pronounced, and the system no longer provides selective amplification (dark red and dark blue). A careful inspection of the data reveals a slight drop in the response of resonator i at the resonance frequency of resonator j for low excitation amplitudes. This effect results from the physical coupling between the two resonators through their open ends.

Examining the corresponding sensitivity curves in Fig. 2(d), we retrieve the three different regimes in both resonators. For low excitation amplitudes, both resonators exhibit linear amplification of the response, whereas at high excitation levels, the response increases passively, i.e., without amplification. The transition between these two regimes is governed by the cubic nonlinearity of the loop function, leading to a change in the observed slope in the log-log representation: the slope transitions from 1 to 1/3, a characteristic signature of cubic nonlinearity; the gain is represented in the gray-shaded region and is equal to 26 (a full study and more details on the gain are provided in the last section). However, this value corresponds to the same as in Fig. 4 when $G_0 = 1.18$ and $\alpha = 0$. Such sensitivity curves reveal the amplification of the low-amplitudes, similar to the cochlear amplifier in the inner ear (Martin and Hudspeth, 2001; Barral and Martin, 2012).

This behavior serves as a reference case before introducing coupling ($\alpha \neq 0$), which will modify the response of both resonators.

When the coupling is activated and α is increased to 0.2 [Fig. 2(b)], we observe significant modifications in the resonators' responses. First, a shift in the resonance frequencies occurs at low excitation amplitudes: the frequency of the first resonator increases from 907 to 916 Hz, while that of the second resonator decreases from 973 to 965 Hz. This shift indicates the onset of coupling-induced interactions between the resonators. Second, the resonance peaks at low amplitudes appear broader and less sharp compared to the uncoupled case ($\alpha = 0$). This effect is quantitatively reflected in the corresponding sensitivity curve [Fig. 2(e)], which shows a reduced gain in the gray-shaded region, indicating the intermediate regime between the two linear behaviors observed at low and high amplitudes. The gain decreases from 26 to 15, which is the data point in Fig. 4 for $G_0 = 1.18$ and $\alpha = 0.2$. As a result, the inverse cubic

regime, characteristic of the cubic nonlinearity, is less pronounced than in the uncoupled case.

As the coupling parameter is further increased to its maximum value, $\alpha = 1$, where the resonator is exclusively coupled to its neighbor, we observe a striking phenomenon: the two resonance peaks fully merge at low excitation amplitudes, forming a single resonance, as shown in Fig. 2(c). This merged resonance occurs at 939 Hz, a frequency approximately midway between the natural frequencies of the uncoupled resonators. The corresponding sensitivity curve in Fig. 2(f) further supports this observation, revealing that the gain in the intermediate regime (shaded gray region) has nearly returned to its original value, reaching 25. This point is represented in Fig. 4 for $G_0 = 1.18$ and $\alpha = 1$.

IV. DISCUSSION

A. Syncrhonization

To further analyze the merging of resonance frequencies, Fig. 3 presents the experimental results from a different perspective, showing the maximum of the response amplitude as a function of frequency, focusing specifically on how the resonance frequencies of the two resonators evolve as the coupling coefficient α increases. At low excitation amplitudes, the two frequencies gradually approach each other (see the response in light red and blue), while at higher excitation amplitudes, they revert to their original uncoupled values (see dark red and blue). This behavior is characteristic of nonlinear synchronization (Pikovsky *et al.*, 2003; Strogatz, 2003), where coupled oscillators tend to lock onto a common frequency in a certain parameter range. The observed frequency locking aligns with canonical models of coupled nonlinear oscillators, such as the Kuramoto model and its extensions, which describe how oscillators with different natural frequencies adjust their rhythms through coupling (Kuramoto, 1975; Acebrón *et al.*, 2005). Here, at higher energies, they recover their independent dynamics because the gain function saturates, which limits the feedback strength and consequently leads to the suppression of both nonlinearity and coupling.

In the absence of coupling ($\alpha = 0$), as shown in Fig. 3(a), the resonance frequencies remain fixed at their natural values, $f_1 = 907$ Hz and $f_2 = 973$ Hz, for all excitation amplitudes, indicating no interaction between the resonators. As coupling is introduced [$\alpha = 0.2$, Fig. 3(b)], the frequencies start to converge, shifting to $f_1 = 916$ Hz and $f_2 = 965$ Hz at low excitation levels. However, as the excitation amplitude increases, the frequencies gradually return to their initial uncoupled values. With a stronger coupling of $\alpha = 0.3$ [Fig. 3(c)], the resonance frequencies move even closer, reaching $f_1 = 927$ Hz and $f_2 = 945$ Hz at low excitation. Yet again, as the excitation increases, the system transitions out of the synchronized regime, and the resonance frequencies revert to their original values. At $\alpha = 0.4$ [Fig. 3(d)], the resonance frequencies become nearly identical at low excitation, with $f_1 = 937$ Hz and $f_2 = 939$ Hz, indicating a near-complete synchronization of the two resonators. However, as the excitation amplitude increases, the system departs from the synchronized state, and the frequencies separate again. Finally, at maximum coupling ($\alpha = 1$) [Fig. 3(e)], the two frequencies fully merge at low excitation amplitudes, forming a single resonance at $f_1 = f_2 = 939$ Hz. This corresponds to a complete synchronization of the two resonators in this regime. As the excitation intensity increases, gain saturation weakens both nonlinear amplification and inter-resonator coupling, breaking the synchronization and restoring the original frequency separation.

In summary, increasing α enhances the coupling strength and progressively brings the resonance frequencies closer together, ultimately leading to frequency synchronization at low amplitudes. However, at higher excitation amplitudes, the system moves out of this synchronized state due to the saturation of the gain function, causing the frequencies to revert to their original values. This behavior highlights a transition from a synchronized regime at low amplitudes to a desynchronized regime at high amplitudes. This transition is consistent with nonlinear oscillator theory,

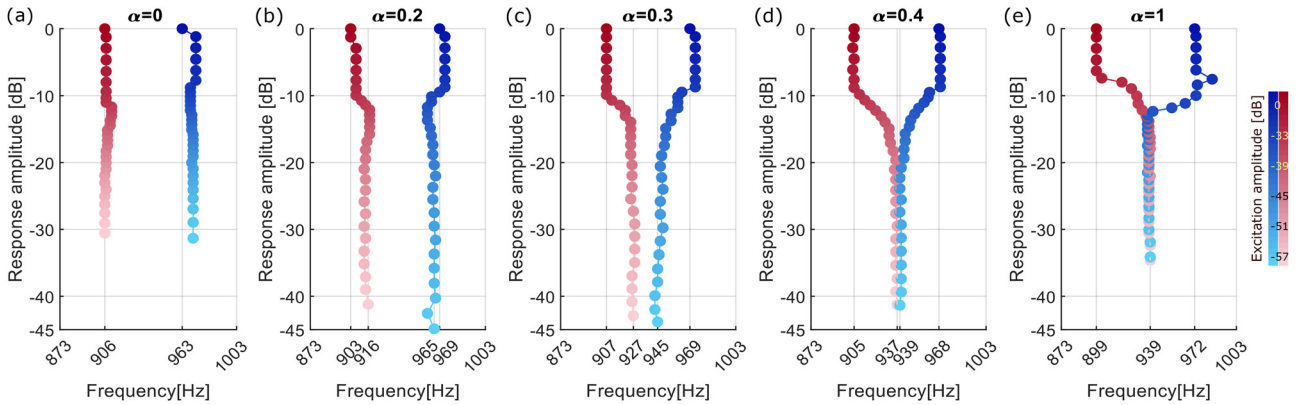

FIG. 3. Synchronization of nonlinear resonators as a function of coupling - Graphs showing the evolution of the resonance frequency in each resonator as a function of excitation amplitude and coupling coefficient. (a) For the uncoupled case ($\alpha = 0$), the resonance frequencies remain constant regardless of excitation level. (b) With weak coupling ($\alpha = 0.2$), the frequencies begin to converge at low excitation but revert to their uncoupled values at high excitation. (c) Increasing the coupling further ($\alpha = 0.3$) narrows the frequency gap at low amplitudes. (d) At intermediate coupling ($\alpha = 0.4$), the frequencies nearly align under low excitation, while (e) under strong coupling ($\alpha = 1$), the resonances merge completely at low amplitudes and return to their initial values at high excitation.

https://doi.org/10.1121/10.0038955

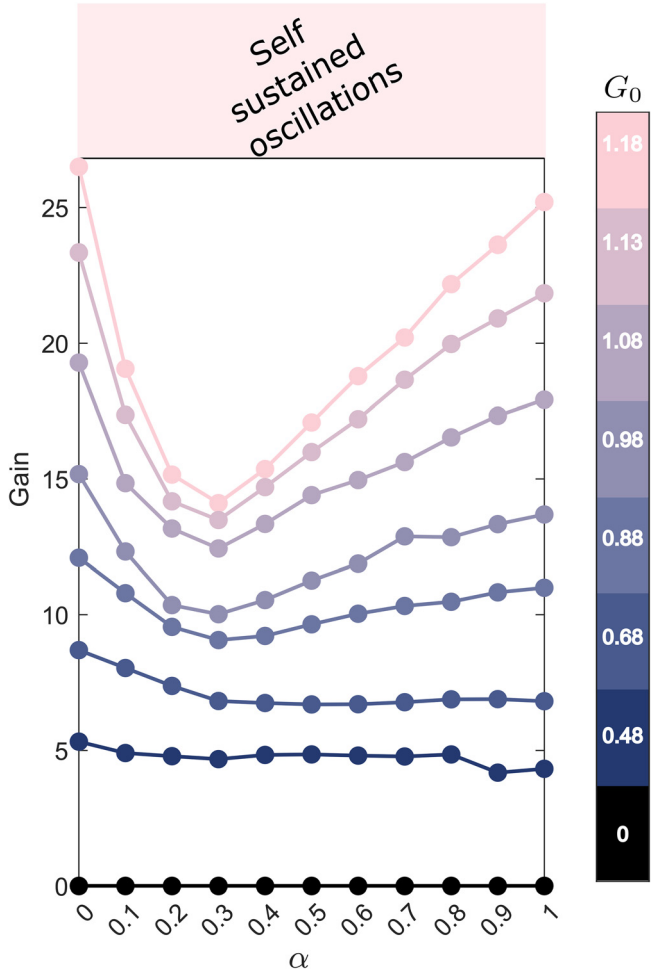

FIG. 4. The dependence of the second resonator's gain on the coupling coefficient α and the variable gain G_0. As G_0 is decreased, the gain at low excitation amplitudes decreases, following a convex shape with a minimum at $\alpha = 0.3$, indicating that the coupled system reaches the threshold for self-sustained oscillations less easily than isolated subsystems. At lower G_0 values, the gain becomes constant. These results demonstrate the interplay between coupling strength and gain. The figure shows the dependence of the second resonator's gain on the coupling coefficient α and the variable gain G_0. As G_0 is decreased, the gain at low excitation amplitudes decreases, following a convex shape with a minimum at $\alpha = 0.3$. Then it becomes constant at lower G_0 values, indicating that the coupled system reaches the threshold for self-sustained oscillations less easily than isolated subsystems. The results demonstrate the interplay between coupling strength and gain.

where the interplay between coupling strength and amplitude-dependent gain determines synchronization stability (Strogatz, 2000; Rosenblum *et al.*, 1996). The synchronization observed in our coupled resonators recalls a landmark historical observation by Christiaan Huygens in 1665 (Huygens, 1665). Huygens noted that two of his pendulum clocks, when mounted on the same wooden beam, gradually synchronized their oscillations in opposite directions—an anti-phase relationship. In his arrangement, the weak mechanical coupling through the shared beam favored a stable configuration in which the pendulums swung out of phase, thereby minimizing the beam's motion and allowing both clocks to run more steadily. Huygens reported that, regardless of their initial states, the pendulums inevitably settled into this synchronized pattern. This "sympathy of clocks" is now recognized as one of the earliest recorded examples of synchronization in coupled oscillators, a concept that has since become central across physics, engineering, biology, and neuroscience. The behavior we observe in our acoustic resonators follows the same principles, where weak coupling leads to a gradual frequency adjustment, which, as the coupling strength reaches its maximum, culminates in full synchronization under specific conditions.

B. Gain

A new series of experiments is motivated by our initial observation that, for the uncoupled resonators ($\alpha = 0$) just below the threshold for self-sustained oscillations, increasing the coupling parameter ($\alpha \neq 0$) leads to a reduction in the amplification of low amplitudes [Figs. 2(b) and 2(e)]. To systematically investigate this effect, we conduct multiple experiments to examine how the system's gain evolves as a function of both the coupling coefficient α and the value of the constant gain G_i. Thus, G_1 and G_2 will also change, but in the same proportion for both. Hence, for the rest of this article, we introduce the parameter G_0 as $G_0 = G_2$ and $G_0 = 1.18\,G_1$, with G_0 being the variable that changes. In this set of experiments, we investigate how the gain of the second resonator, specifically the amplification of low amplitudes, depends on both the parameter G_0 and the coupling coefficient α.

The results, shown in Fig. 4, clearly reveal the dependence of the second resonator's gain on these two parameters. Each time, we emit monochromatic sound waves for one second and measure the pressure inside the tubes, thus exciting the system in the same monochromatic manner as before. This time, the coupling coefficient α is incrementally varied from $\alpha = 0$ (no coupling) to $\alpha = 1$ (fully coupled), while the parameter G_0 is also decreased.

We selected $G_0 = 1.18$ as the highest value tested since the system enters the oscillatory regime above this threshold for $\alpha = 0$, as we explained. At this level, the gain—quantifying the amplification at low excitation amplitudes—was measured at 26 for $\alpha = 0$ and slightly decreased to 25 at $\alpha = 1$. The variation in gain follows a convex shape, reaching a minimum value of 14 at an intermediate coupling of $\alpha = 0.3$.

To further probe this effect, we repeat the experiment with a lower G_0 of $G_0 = 1.13$, chosen because it accentuated the observed trends. At this level, the maximum gain at $\alpha = 0$ is 23, decreasing to a minimum of 13 at $\alpha = 0.3$ before recovering to 22 at $\alpha = 1$. This experiment is repeated for five additional values of G_0, each time decreasing G_0 until $G_0 = 0.48$. As G_0 decreases, the convex behavior in the gain becomes progressively weaker, eventually leading to a constant gain equal to almost 5 across all coupling values at $G_0 = 0.48$. At the extreme case of $G_0 = 0$, the gain remains zero, independent of α.

These results highlight the relationship between the coupling strength and the constant gains G_i. The gain exhibits a non-monotonic dependence on α, with a marked suppression at intermediate coupling values ($\alpha \approx 0.3$),

followed by a recovery at stronger coupling. As G_0 decreases, this non-monotonic trend fades, and the gain becomes independent of α. This behavior shows that a coupled system, depending on its coupling, can reach the threshold for self-sustained oscillations less easily than two isolated subsystems, specifically for $\alpha = 0.3$, where the system is particularly less sensitive to perturbations.

V. CONCLUSION

Our investigation into the nonlinear coupling dynamics between two delayed acoustic resonators has deepened our understanding of complex resonator interactions. By varying the coupling coefficient and systematically adjusting the feedback gain, we observed frequency synchronization at low excitation amplitudes and desynchronization at higher ones. At low amplitudes, the resonance frequencies of the coupled resonators converged, while at higher amplitudes, they remained close to their intrinsic values, demonstrating the critical interplay between coupling strength and nonlinear response. The experiments also underscored the fundamental role of the constant gain, G_0, and the coupling coefficient, α, in shaping resonator behavior, particularly when operating near the threshold for self-sustained oscillations in the uncoupled system. Full synchronization—occurring just before the reemergence of self-sustained oscillations—was observed only at maximum coupling. This work, building on our previous exploration of Hopf resonators mimicking the cochlear amplifier (Reda *et al.*, 2023), offers valuable insights into the nonlinear dynamics of coupled systems.

The digital coupling that synchronized the resonators' frequencies exemplifies how chaotic systems can transition into coherent states, reflecting a broader phenomenon in nature where disorder often gives way to spontaneous order. From Huygens' pendulums to synchronized firefly flashes, planetary orbits, and neuronal oscillations, these examples of synchronization reveal a fundamental principle of coherence in both biological and physical systems. While the cochlea relies on passive mechanical coupling (Ranke, 1950; Weiss, 1982; Jean *et al.*, 2020), our system implements nonlinear coupling via active digital feedback.

This study not only advances our understanding of nonlinear coupling in acoustic delayed systems but also lays the groundwork for future research into resonator dynamics, acoustic signal processing applications, and simulations of auditory mechanisms. The integration of digital feedback and nonlinear gain modulation in our experimental framework marks a key step toward designing controllable acoustic systems that emulate the cochlear amplifier.

ACKNOWLEDGMENTS

This work has received support under the program "Investissements d'Avenir" launched by the French Government and by the Simons Foundation/Collaboration on Symmetry-Driven Extreme Wave Phenomena.

AUTHOR DECLARATIONS

Conflict of Interest

The authors have no conflicts to disclose.

DATA AVAILABILITY

The data that support the findings of this study are available from the corresponding author upon reasonable request.

Acebrón, J. A., Bonilla, L. L., Vicente, C. J. P., Ritort, F., and Spigler, R. (**2005**). "The Kuramoto model: A simple paradigm for synchronization phenomena," Rev. Mod. Phys. **77**(1), 137–185.

Barral, J., and Martin, P. (**2012**). "Phantom tones and suppressive masking by active nonlinear oscillation of the hair-cell bundle," Proc. Natl. Acad. Sci. U.S.A. **109**(21), E1344–E1351.

Brunet, T., Merlin, A., Mascaro, B., Zimny, K., Leng, J., Poncelet, O., Aristégui, C., and Mondain-Monval, O. (**2015**). "Soft 3D acoustic metamaterial with negative index," Nat. Mater. **14**, 384–388.

Craster, R. V. (**2024**). *Acoustic Metamaterials: Absorption, Cloaking, Imaging, Time-Modulated Media, and Topological Crystals* (Springer Nature, New York), Vol. 345.

Crauste, F. (**2009**). "Delay model of hematopoietic stem cell dynamics: Asymptotic stability and stability switch," Math. Model. Nat. Phenom. **4**(2), 28–47.

Cummer, S. A., Christensen, J., and Alù, A. (**2016**). "Controlling sound with acoustic metamaterials," Nat. Rev. Mater. **1**(3), 16001.

Duke, T., and Jülicher, F. (**2003**). "Active traveling wave in the cochlea," Phys. Rev. Lett. **90**(15), 158101.

Gomez, F., Lorimer, T., and Stoop, R. (**2016**). "Signal-coupled subthreshold Hopf-type systems show a sharpened collective response," Phys. Rev. Lett. **116**, 108101.

Hamilton, M. F. (**1986**). *Fundamentals and Applications of Nonlinear Acoustics* (ASME, New York), pp. 1–28.

Huygens, C. (**1665**). "Letter on the 'sympathy of clocks' (26–27 February 1665)," Letter to Robert Moray and Constantijn Huygens, Oeuvres Complètes de Christiaan Huygens 5, 246, available at https://www.dbnl.org/tekst/huyg003oeuv05_01/huyg003oeuv05_01_0141.php, original letter dated February 27, 1665.

Jean, P., Anttonen, T., Michanski, S., de Diego, A. M., Steyer, A. M., Neef, A., Oestreicher, D., Kroll, J., Nardis, C., Pangršič, T., Möbius, W., Ashmore, J., Whicmann, C., and Moser, T. (**2020**). "Macromolecular and electrical coupling between inner hair cells in the rodent cochlea," Nat. Commun. **11**(1), 3208.

Jiménez, N., Romero-García, V., Pagneux, V., and Groby, J.-P. (**2017**). "Rainbow-trapping absorbers: Broadband, perfect and asymmetric sound absorption by subwavelength panels for transmission problems," Sci. Rep. **7**(1), 13595.

Kaina, N., Lemoult, F., Fink, M., and Lerosey, G. (**2015**). "Negative refractive index and acoustic superlens from multiple scattering in single negative metamaterials," Nature **525**(7567), 77–81.

Kuramoto, Y. (**1975**). "Self-entrainment of a population of coupled nonlinear oscillators," in *Proceedings of the International Symposium on Mathematical Problems in Theoretical Physics*, pp. 420–422.

Lemoult, F., Fink, M., and Lerosey, G. (**2011**). "Acoustic resonators for far-field control of sound on a subwavelength scale," Phys. Rev. Lett. **107**(6), 064301.

Lemoult, F., Kaina, N., Fink, M., and Lerosey, G. (**2016**). "Soda cans metamaterial: A subwavelength-scaled phononic crystal," Crystals **6**(7), 82.

Marsden, J. E., and McCracken, M. (**2012**). *The Hopf Bifurcation and Its Applications*, 19 (Springer Science & Business Media, New York).

Martin, P., and Hudspeth, A. (**2001**). "Compressive nonlinearity in the hair bundle's active response to mechanical stimulation," Proc. Natl. Acad. Sci. U.S.A. **98**(25), 14386–14391.

Meng, H., Chronopoulos, D., Fabro, A., Elmadih, W., and Maskery, I. (**2020**). "Rainbow metamaterials for broadband multi-frequency vibration attenuation: Numerical analysis and experimental validation," J. Sound Vib. **465**, 115005.

Ni, X., Wu, Y., Chen, Z.-G., Zheng, L.-Y., Xu, Y.-L., Nayar, P., Liu, X.-P., Lu, M.-H., and Chen, Y.-F. (**2014**). "Acoustic rainbow trapping by coiling up space," Sci. Rep. **4**(1), 7038.
Nin, F., Reichenbach, T., Fisher, J. A. N., and Hudspeth, A. J. (**2012**). "Contribution of active hair-bundle motility to nonlinear amplification in the mammalian cochlea," Proc. Natl. Acad. Sci. U.S.A. **109**(51), 21076–21080.
Pikovsky, A., Rosenblum, M., and Kurths, J. (**2003**). *Synchronization: A Universal Concept in Nonlinear Sciences* (Cambridge University Press, Cambridge, UK).
Plaçais, P.-Y., Balland, M., Guérin, T., Joanny, J.-F., and Martin, P. (**2009**). "Spontaneous oscillations of a minimal actomyosin system under elastic loading," Phys. Rev. Lett. **103**, 158102.
Ranke, O. F. (**1950**). "Theory of operation of the cochlea: A contribution to the hydrodynamics of the cochlea," J. Acoust. Soc. Am. **22**(6), 772–777.
Reda, J., Fink, M., and Lemoult, F. (**2023**). "A non-linear delayed resonator for mimicking the hearing haircells," Europhys. Lett. **144**(3), 37001.
Rosenblum, M. G., Pikovsky, A. S., and Kurths, J. (**1996**). "Phase synchronization of chaotic oscillators," Phys. Rev. Lett. **76**(11), 1804–1807.
Rupin, M., Lerosey, G., de Rosny, J., and Lemoult, F. (**2019**). "Mimicking the cochlea with an active acoustic metamaterial," New J. Phys. **21**(9), 093012.
Strogatz, S. H. (**2000**). "From Kuramoto to Crawford: Exploring the onset of synchronization in populations of coupled oscillators," Phys. D **143**(1-4), 1–20.
Strogatz, S. H. (**2003**). *Sync: The Emerging Science of Spontaneous Order* (Penguin, London, UK).
Tian, Z., and Yu, L. (**2017**). "Rainbow trapping of ultrasonic guided waves in chirped phononic crystal plates," Sci. Rep. **7**(1), 40004.
Weiss, T. (**1982**). "Bidirectional transduction in vertebrate hair cells: A mechanism for coupling mechanical and electrical processes," Hear. Res. **7**(3), 353–360.
Zhu, J., Chen, Y., Zhu, X., Garcia-Vidal, F. J., Yin, X., Zhang, W., and Zhang, X. (**2013**). "Acoustic rainbow trapping," Sci. Rep. **3**(1), 1728.